Journal of Engineering Mathematics **41:** 75–99, 2001.

Stokes flow in a mixer with changing geometry

MATTHEW D. FINN and STEPHEN M. COX
School of Mathematical Sciences, University of Nottingham, University Park, Nottingham NG7 2RD, United Kingdom
E-mail: pmxmdf@thmech.nottingham.ac.uk; stephen.cox@nottingham.ac.uk

Received 11 September 2000; accepted in revised form 2 May 2001

Abstract. A slow-flow mixing device that mimics a natural mixing technique is described. Analytical, numerical and experimental results are presented for the 'translating, rotating mixer', which illustrate its mixing effectiveness. In large part, this effectiveness is due to the fact that its geometry changes with time, a feature rare in mathematically tractable slow-flow mixing models. The mixer consists of a large circular cylinder filled with fluid, which is stirred by a circular cylindrical 'rod' that moves around in the fluid. The stirring rod may also rotate about its axis. The velocity field is calculated explicitly for the mixer, and its mixing action is simulated numerically. Through a complex-variable formulation of the problem, the energy input required for various mixing protocols may readily be determined, and in turn suggestions for efficient mixing using the device are offered. To validate the analytical and numerical results, tracer-advection experiments are performed, using a simple experimental rig and a variety of mixing protocols, providing encouraging agreement with numerical simulation.

Key words: Stokes flow, laminar mixing, biharmonic equation, image systems.

1. Introduction

Fluid mixing is a problem that is widely encountered, from everyday examples such as the stirring of milk into a mug of coffee, to large-scale processes in the chemical engineering industry. In this paper, we describe through analysis, numerics and experiment a simple mixing device that mimics a natural technique for mixing.

Our mixing device consists of a circular cylindrical vat inside which fluid is stirred by a rod of circular cross-section, which may be moved in an arbitrary motion across the vat of fluid. In addition, the stirring rod may also be 'twirled', *i.e.*, rotated about its own axis, and the vat itself may be rotated about its axis. By making the slow-flow approximation (that the Reynolds number of the flow is vanishingly small), we are able to compute the flow field exactly, and this greatly facilitates our numerical simulations of the mixing (see [1] for a warning against using approximate expressions for the flow field).

The slow-flow approximation is relevant for a range of engineering processes in which delicate molecules (such as long-chain polymers or bio-molecules) are to be mixed. For example, it is well known that the large shear rates associated with turbulent mixers cause undesirable damage to proteins, micro-organisms, animal and plant cells: this is a major problem in bioprocess engineering (see the review by Thomas [2], for example). Despite the flow in our mixer being laminar, we shall demonstrate that, in common with other mixers where the velocity field is chaotic [3, 4], it is capable of excellent mixing. To validate our results, we perform some experiments using our mixing device.

Although there have been many previous descriptions of slow-flow mixers, these have almost exclusively concerned devices with a fixed geometry (a notable exception is the mixing

device of Jana et al. [5]; in addition, one could argue that the blinking rotlet flow of Meleshko and Aref [6] involves a changing geometry, because the singularities in the flow field that drive the motion alternate between two positions). The key novel feature of our mixing device is that the geometry of the flow domain changes with time as the stirring rod moves around. As we demonstrate below, this feature, which is found in virtually any mixer that relies upon moving parts, makes the mixer highly effective.

Our mixing device, which we call the TRM (translating, rotating mixer) significantly improves upon the much studied EAM (eccentric annular mixer) [7–18], in which fluid is also contained between two non-concentric circular cylinders with parallel axes. In the EAM, however, stirring of the fluid is achieved only by a rotation of the outer and inner cylinders about their respective axes (the inner cylinder in the EAM thus represents a stirring rod whose axis is fixed, but which is free to rotate about this fixed axis). If this rotation is carried out in a time-dependent fashion, the fluid may undergo chaotic motion with consequently good mixing. In the TRM, the inner cylinder is also free to move laterally, so that the geometry of the flow domain evolves with time, leading to better mixing and a better model for the behaviour of real mixing devices.

The streamfunction for the flow satisfies the biharmonic equation. Since this equation and the imposed boundary conditions are linear, we may assemble the velocity field for the TRM by adding together the appropriate solutions corresponding to the various components of the motion. Several of the necessary solutions already exist in the literature, and others have been derived in special cases, but the general translational motion of the stirring rod has not been given before. We now briefly summarise these special cases and individual elements of the TRM flow.

The flow field for the EAM (*i.e.*, for the twirling of the stirring rod, and for the rotation of the outer wall of the vat) was first given by Jeffery [14] in bipolar coordinates; this work was later extended [7, 11, 15]. The solution in Cartesian coordinates was first given by Wannier [18], who calculated the flow field together with the forces and moments acting on the boundaries. The translational component of the motion has been solved in two special cases [19–21], but not for general motion of the stirring rod. (A plane elastic problem analogous to translation of the inner cylinder has also been solved, in bipolar coordinates, by Stevenson [22], following earlier work of Jeffery [23] – see also Milne-Thomson [24].) In the special case in which the outer cylinder has infinite radius (*i.e.*, it becomes a plane wall), Jeffrey and Onishi [25] obtained the flow due to a translating and rotating inner cylinder. This work has been of particular value in providing an asymptotic check on our analytical results. Forces and moments on the inner cylinder were computed by Jeffrey and Onishi [25], with experimental confirmation of the Stokes drag given by Trahan and Hussey [26].

In deriving the velocity field for flow in the TRM, we make use of the method of images for slow flow inside a circular boundary. We summarise the method of images in complex-variable form in Section 2, and illustrate its application to two simple singularities: a rotlet and a (modified) stokeslet, the former example giving a more direct derivation of the rotlet flow of Meleshko and Aref [6]. The energetics of the motion are considered in Section 3. The rotlet and the modified stokeslet, together with their image singularities, form the basis of the TRM velocity field, which is derived in Section 4, along with a calculation of its associated energetics. Numerical simulations and experiments with the TRM follow in Section 5, showing its mixing effectiveness. We make our concluding remarks in Section 6.

2. Image systems for slow flow inside a circular cylinder

For two-dimensional, slow viscous flow, the streamfunction $\psi(x, y, t)$ that governs the velocity field $(u, v) = (\partial\psi/\partial y, -\partial\psi/\partial x)$ satisfies the biharmonic equation [16, 27]

$$\nabla^4\psi = 0. \tag{1}$$

The velocity field is assumed to be quasi-static, meaning that temporal variations in the velocity field are slow enough that the time derivative term in the Navier–Stokes equations may be ignored in deriving (1).

To calculate the velocity field for the translating, rotating mixer, we shall make use of the method of images in a circular boundary at which both components of the fluid velocity vanish. We therefore begin by discussing, in this section, this method of images. Readers not interested in the derivation of the velocity field may skip directly to Section 4.5.

For flow in a domain between a pair of non-concentric circular boundaries, it seems natural to work in bipolar coordinates. However, we prefer a complex-variable formulation, which is essentially based on Cartesian coordinates. The first reason is that the flow field may readily be computed in finite terms in this coordinate system; the second is a practical issue that our numerical simulations are most conveniently carried out in Cartesian coordinates.

The full streamfunction for the TRM is composed of various singular solutions to (1), together with their images in the outer circular boundary (none of the singularities lies in the flow domain). In general, singular solutions to (1) are useful in generating flows past bodies of various geometries (see, for example, Chwang and Wu [19] and the review by Hasimoto and Sano [28]). In particular it is useful to know, given a singularity, the corresponding system of images in a no-slip boundary. The first such treatment of images for the biharmonic equation was given by Lorentz [29], for images in a rigid plane boundary. The images of the basic singular solutions (stokeslet, rotlet, source, doublet) in such a boundary were later catalogued by a variety of authors [30–34].

The corresponding method of images for a no-slip *circular* boundary [35, 36] seems to have developed in a rather more ad hoc fashion. A method of images was first sketched by Frazer [20]. Two equivalent 'circle theorems' [37, 38] have since been derived for flow *exterior* to a no-slip circular boundary. In each case, the method for constructing the appropriate images makes use of the result of Michell [39] on inversion of solutions to the biharmonic equation in a circle. However, our interest lies rather with the interior flow, inside a circular boundary.

We present below a method of images for flow inside a rigid circular cylinder with a no-slip boundary. Our procedure is rather more systematic than, for example, that used by Avudainayagam and Jothiram [35], who constructed the streamfunction due to a rotlet outside a circle from the original rotlet singularity together with other singularities, whose magnitudes were determined by applying the outer boundary condition. Ranger [34] has carried out a corresponding calculation for flow due to a rotlet inside a circle. As with the Milne-Thomson circle theorem for *inviscid* flow [27], extraneous images may be introduced at the origin through a naive calculation of the image system. These must be removed: our procedure for doing so is Frazer's 'method of successive reflections' [20], which we describe below.

We introduce the complex coordinates

$$z = x + \mathrm{i}y, \quad \bar{z} = x - \mathrm{i}y \tag{2}$$

(throughout this paper, the overbar will denote complex conjugation), in terms of which the biharmonic equation (1) becomes [22]

$$\frac{\partial^4 \psi}{\partial^2 z \, \partial^2 \bar{z}} = 0. \tag{3}$$

The general solution to (3) may be written in the form [27]

$$\psi(z, \bar{z}) = \bar{z} f(z) + z \bar{f}(\bar{z}) + g(z) + \bar{g}(\bar{z}), \tag{4}$$

where f and g are arbitrary differentiable functions, with the corresponding velocity field (u, v) being given by

$$u + \mathrm{i}v = -2\mathrm{i}\frac{\partial \psi}{\partial \bar{z}}. \tag{5}$$

The major result that we use in determining the image system in a no-slip circular boundary is the following. We suppose that a streamfunction $\psi(z, \bar{z})$ of the form (4) has a given set of singularities, none of which lie on the circle $|z| = a$. Then the streamfunction

$$\begin{aligned} \Psi(z, \bar{z}) \; = \; & \bar{z} f(z) + z \bar{f}(\bar{z}) + g(z) + \bar{g}(\bar{z}) - z \bar{f}(a^2/z) - \bar{z} f(a^2/\bar{z}) - \bar{g}(a^2/z) - g(a^2/\bar{z}) \\ & + (a^2 - |z|^2) \left\{ \bar{f}'(a^2/z) + f'(a^2/\bar{z}) + z^{-1} \bar{g}'(a^2/z) + \bar{z}^{-1} g'(a^2/\bar{z}) \right\} \end{aligned} \tag{6}$$

satisfies the no-slip boundary condition

$$u + \mathrm{i}v = 0 \qquad \text{on } |z| = a, \tag{7}$$

and has the same set of singularities inside $|z| = a$ as does ψ, except possibly for additional singularities at the origin $z = 0$, due to the terms in $a^2 z^{-1}$ and $a^2 \bar{z}^{-1}$ in (6). Furthermore, $\Psi = 0$ on $|z| = a$ (this rather convenient feature justifies some of the constants that we keep when deriving streamfunctions below, that one might otherwise discard). The locations of the singularities of Ψ are those of the original streamfunction ψ, together with their images in the circle $|z| = a$ (including the image of the point at infinity). By analogy with (4), Ψ may be written in the form

$$\Psi = \bar{z} F(z) + z \bar{F}(\bar{z}) + G(z) + \bar{G}(\bar{z}), \tag{8}$$

where

$$F(z) \; = \; f(z) - z \bar{f}'(a^2/z) - \bar{g}'(a^2/z), \tag{9}$$

$$G(z) \; = \; g(z) - z \bar{f}(a^2/z) + a^2 \bar{f}'(a^2/z) - \bar{g}(a^2/z) + a^2 z^{-1} \bar{g}'(a^2/z), \tag{10}$$

these functions being just the 'conjugate functions' of Frazer [20][1].

To remove any (unphysical) singularities introduced at the origin in the derivation of Ψ from ψ, we apply a modified version of Frazer's method of successive reflections [20], as follows. We first investigate the singularities of Ψ as $z \to 0$, then generate their images in the circle $|z| = a$, finally subtracting off an appropriate multiple of the result from Ψ. At least for singularities of the form z^{-n} or $z^n \log z$, this process will be successful in removing spurious singularities from Ψ at the origin, as illustrated below in Section 2.1 and 2.2.

[1]The corresponding formulas for images in the plane $y = 0$ are $F(z) = f(z) - z\bar{f}'(z) - \bar{g}'(z)$ and $G(z) = g(z) - z\bar{f}(z) + z^2 \bar{f}'(z) - \bar{g}(z) + z\bar{g}'(z)$ [20]. These expressions are based on the plane image method of Lorentz [29].

We now demonstrate how the method of images is applied to two singularities: the rotlet and the modified stokeslet. These will form the basic building blocks for our construction of the TRM streamfunction, in Section 4 below.

2.1. THE IMAGE SYSTEM FOR THE ROTLET

In this subsection, we apply the method of images to a rotlet placed inside the boundary $|z| = a$, at the point $z = s \in \mathfrak{R}$. The resulting flow has been derived elsewhere by different methods, by Ranger [34] and by Meleshko and Aref [6]. Ranger's approach is based on a limiting case of the solution of Jeffery [14] for the EAM; it allows the outer boundary to rotate, although we defer consideration of this feature to later. Meleshko and Aref [6] use a Fourier series to calculate the images of the rotlet; the following method is rather simpler and more direct than theirs.

We consider the streamfunction

$$\psi = C \log|z - s| = \tfrac{1}{2}C\{\log(z - s) + \log(\bar{z} - s)\}, \tag{11}$$

where $C \in \mathfrak{R}$, for a rotlet of strength C. The corresponding functions f and g in (4) are then

$$f(z) = 0, \quad g(z) = \tfrac{1}{2}C \log(z - s), \tag{12}$$

and the corresponding image system obtained from (9) and (10) is

$$F(z) = \frac{Cz}{2s(z - \sigma)}, \quad G(z) = \frac{C}{2}\left\{\log\left(-\frac{z - s}{s(z - \sigma)}\right) - \frac{\sigma}{z - \sigma} + \log z\right\}, \tag{13}$$

where $s\sigma = a^2$. The streamfunction Ψ generated by substituting (13) in (8) then satisfies the no-slip boundary condition on $|z| = a$, but has an unphysical logarithmic singularity at the origin which is not present in the original streamfunction ψ given by (11). In physical terms, this singularity is removed as follows. We note first that simply subtracting the offending logarithm (*i.e.* rotlet) from $G(z)$ would induce a tangential slip velocity on the cylinder wall $|z| = a$, which would violate the no-slip condition there. This condition can, however, be reinstated by adding to the system of singularities a rigid body rotation about the origin.

To see mathematically how this procedure is accomplished, we consider the image of the offending singularity in $|z| = a$, given by taking a streamfunction of the form (4), with

$$f(z) = 0, \quad g(z) = P \log z. \tag{14}$$

According to (9) and (10), we find the corresponding image system to be given by a streamfunction of the form (8), with

$$F(z) = -\bar{P}za^{-2}, \quad G(z) = \bar{P}(1 - \log a^2) + (P + \bar{P}) \log z. \tag{15}$$

It follows from (13) and (15) that, in order to eliminate the singularity in Ψ at the origin, we must add to the functions in (12) the functions in (14), with $P = -\frac{1}{4}C$. If we do so and use (8), we arrive at the final streamfunction

$$\Psi = \frac{C}{2}\left\{\log\frac{\sigma|z - s|^2}{s|z - \sigma|^2} + \frac{(|z|^2 - a^2)(|z|^2 - \sigma^2)}{a^2|z - \sigma|^2}\right\}, \tag{16}$$

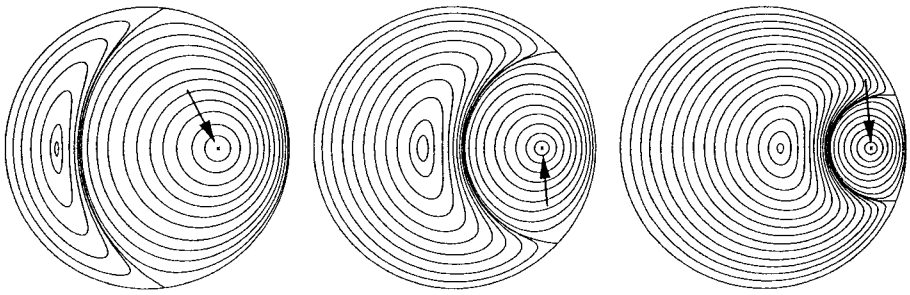

Figure 1. Streamlines corresponding to a rotlet and its image system in the circle $|z| = a$, from (16). From left to right the rotlet locations are $z/a = 4/8, 5/8, 6/8$ (indicated by the arrows).

which is precisely the rotlet flow derived by Ranger [34] and by Meleshko and Aref [6], its only singularity inside the circle $|z| = a$ being at $z = s$. Typical streamlines are shown in Figure 1. In this and all subsequent streamline plots, the streamlines do not represent equispaced values of the streamfunction, but are instead chosen to illustrate the flow pattern.

2.2. The image system for the modified stokeslet

We now turn to the image system associated with a stokeslet placed inside the circle $|z| = a$, at the point $z = s \in \Re$. In fact, it is more convenient to consider a modified stokeslet, which contains only the singular part of the streamfunction, in the form

$$\begin{aligned}\psi &= \tfrac{1}{2}\{A(z+\bar{z}) - \mathrm{i}B(z-\bar{z})\}\log|z-s| \\ &= \tfrac{1}{4}\{(A-\mathrm{i}B)z + (A+\mathrm{i}B)\bar{z}\}\{\log(z-s) + \log(\bar{z}-s)\}, \end{aligned} \tag{17}$$

where A and B are real constants, and $A + \mathrm{i}B$ is the strength of the stokeslet. (Note that an *unmodified* stokeslet [19] would have the logarithm that appears in the first line of (17) replaced by $\log|z-s| - 1$.) Thus in (4),

$$f(z) = \tfrac{1}{4}(A+\mathrm{i}B)\log(z-s), \quad g(z) = \tfrac{1}{4}(A-\mathrm{i}B)z\log(z-s). \tag{18}$$

Substitution in (9) and (10) then yields

$$F(z) = \tfrac{1}{4}(A+\mathrm{i}B)\left\{\log\left(-\frac{z-s}{s(z-\sigma)}\right) + \frac{\sigma}{z-\sigma} + \log z\right\} + \tfrac{1}{4}(A-\mathrm{i}B)\frac{z^2}{s(z-\sigma)}, \tag{19}$$

$$\begin{aligned} G(z) &= \tfrac{1}{4}(A+\mathrm{i}B)\left\{-\frac{a^2}{z-\sigma} + \frac{a^2}{z}\right\} \\ &\quad + \tfrac{1}{4}(A-\mathrm{i}B)\left\{z\log\left(-\frac{z-s}{s(z-\sigma)}\right) - \frac{\sigma z}{z-\sigma} + z\log z\right\}, \end{aligned} \tag{20}$$

with consequent singular behaviour at the origin of the form

$$F(z) \sim \tfrac{1}{4}(A+\mathrm{i}B)\log z, \quad G(z) \sim \tfrac{1}{4}(A+\mathrm{i}B)a^2 z^{-1} + \tfrac{1}{4}(A-\mathrm{i}B)z\log z. \tag{21}$$

To remove these singular parts of the solution, we apply the method of successive reflections [20] as above in Section 2.1, and consider the image of a singular streamfunction of the form (4) with

$$f(z) = P\log z, \quad g(z) = Qz\log z + Rz^{-1}, \tag{22}$$

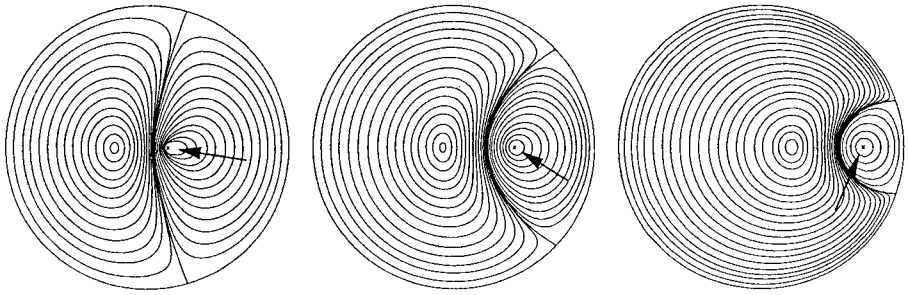

Figure 2. Streamlines corresponding to a modified stokeslet with real strength and its image system in the circle $|z| = a$, from (29). From left to right the stokeslet locations are $z/a = 1/7, 3/7, 5/7$ (indicated by the arrows).

where P, Q and R are complex constants. The image of this system of singularities is given by (9) and (10) to be

$$F(z) = -\bar{Q}(1 + \log a^2) + (\bar{R}a^{-2} - \bar{P})a^{-2}z^2 + (P + \bar{Q})\log z, \tag{23}$$

$$G(z) = \{\bar{P}(1 - \log a^2) - 2\bar{R}a^{-2}\}z + (\bar{P} + Q)z\log z + (\bar{Q}a^2 + R)z^{-1}. \tag{24}$$

It follows that to remove the singular behaviour indicated in (21) we must add to the functions f and g in (18) the functions in (22) with P, Q and R satisfying

$$\tfrac{1}{4}(A + \mathrm{i}B) + P + \bar{Q} = 0, \tag{25}$$

$$\tfrac{1}{4}(A - \mathrm{i}B) + \bar{P} + Q = 0, \tag{26}$$

$$\tfrac{1}{4}(A + \mathrm{i}B)a^2 + \bar{Q}a^2 + R = 0. \tag{27}$$

The solution to this system of equations is clearly not unique since (25) is the complex conjugate of (26), and so we have only two independent equations for three unknowns. However, the streamfunction that results from any combination of P, Q and R satisfying (25)–(27) *is* unique, and a convenient choice is

$$P = 0, \quad Q = -\tfrac{1}{4}(A - \mathrm{i}B), \quad R = 0. \tag{28}$$

The non-uniqueness in the choice of P, Q and R reflects the freedom to decompose a given streamfunction in infinitely many ways into a corresponding $f(z)$ and $g(z)$ (for example, we may replace f and g by $f + 1$ and $g - z$, respectively, without affecting the resulting streamfunction.) Finally, the streamfunction consisting of the modified stokeslet and its images, free of unphysical singularity at the origin is, from (8),

$$\begin{aligned}\Psi = {} & \tfrac{1}{4}\{A(z + \bar{z}) - \mathrm{i}B(z - \bar{z})\}\log\frac{\sigma|z - s|^2}{s|z - \sigma|^2} \\ & + \frac{A(|z|^2 - a^2)}{4s}\left\{\frac{z + s}{z - \sigma} + \frac{\bar{z} + s}{\bar{z} - \sigma}\right\} + \frac{\mathrm{i}B(z - \bar{z})(\sigma - s)(|z|^2 - a^2)}{4s|z - \sigma|^2}.\end{aligned} \tag{29}$$

Typical streamlines for modified-stokeslet image systems with real and imaginary strengths, respectively, are shown in Figures 2 and 3. The form of the streamlines near each kind of

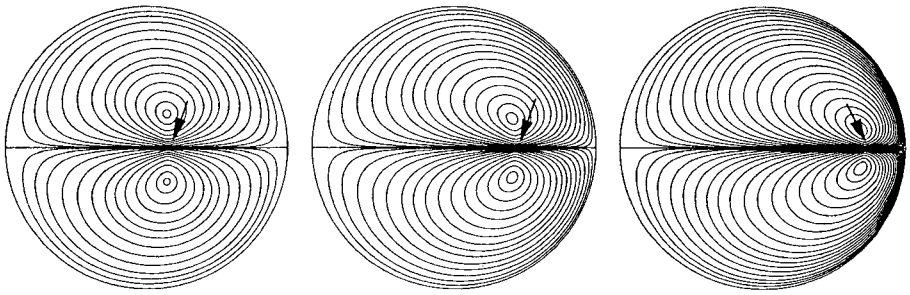

Figure 3. Streamlines corresponding to a modified stokeslet with imaginary strength and its image system in the circle $|z| = a$, from (29). From left to right the stokeslet locations are $z/a = 1/7,\ 3/7,\ 5/7$ (indicated by the arrows).

modified stokeslet is readily confirmed by a local analysis of the streamfunction (*cf.* Figure 1 of [33]).

3. Energetics

The complex-variable formulation of the streamfunction allows us readily to calculate the forces and moments acting on the boundary cylinders. The method is based on that of Stevenson [22] (see also Milne-Thomson [27] and Pozrikidis [40]), and is included here for completeness.

3.1. Background

Let $\mathcal{C}$ denote a boundary whose outward normal points into the fluid, and let the force on this boundary due to the fluid motion be represented by the complex quantity $\mathcal{F}$, where the real and imaginary parts of $\mathcal{F}$ give, respectively, the x- and y-components of the force. Then if the streamfunction for the motion is as in (8), the force on the boundary, per unit length in z, is given by [22, 27]

$$\mathcal{F} = 4\mu \left[-F(z) + z\bar{F}'(\bar{z}) + \bar{G}'(\bar{z}) \right]_{\mathcal{C}}, \tag{30}$$

where $[\, H(z) \,]_{\mathcal{C}}$ is the change in the value of $H(z)$ upon navigating $\mathcal{C}$ once in an anticlockwise sense. Similarly, the moment $\mathcal{M}$ about the origin of the boundary forces acting on $\mathcal{C}$ is [22, 27], per unit length in z,

$$\mathcal{M} = 4\mu\, \Im \left[z\bar{z}\bar{F}'(\bar{z}) + \bar{z}\bar{G}'(\bar{z}) - \bar{G}(\bar{z}) \right]_{\mathcal{C}}. \tag{31}$$

To calculate the corresponding force and moment acting on the outer boundary, we reverse the signs of the expressions (30) and (31).

When calculating the energy requirements of the mixing device, we shall be more interested in the force and moment exerted *on* the fluid *by* the boundaries; these are just the forces and moments described above, with a change of sign.

In the remainder of this section, we calculate the forces and moments generated by various singularities and their associated image systems in a circular boundary. These results are then assembled for the TRM in Section 4.

3.2. THE ENERGETICS OF THE ROTLET

The functions $F(z)$ and $G(z)$ that generate through (8) the streamfunction for the rotlet in the presence of a circular boundary are found by adding together the functions in (13) and (15) with $P = -\frac{1}{4}C$. The force and moment exerted by the cylinder $|z| = a$ on the fluid inside is then found using the results above in Section 3.1, taking the contour $\mathcal{C}$ as the perimeter of the cylinder. Only terms in $F(z)$ and $G(z)$ that are multivalued or have multivalued derivatives may contribute to the force and moment. In a redefinition of notation for the purpose of this calculation, the only relevant components of these functions are

$$F(z) = 0, \quad G(z) = \frac{C}{2}\log\left(-\frac{z-s}{s(z-\sigma)}\right). \tag{32}$$

The resulting forces and moments are then

$$\mathcal{F} = 4\mu\left[\frac{C}{2}\left(\frac{1}{\bar{z}-s} - \frac{1}{\bar{z}-\sigma}\right)\right]_{\mathcal{C}} = 0, \tag{33}$$

$$\begin{aligned}\mathcal{M} &= 4\mu\,\Im\left[\frac{C\bar{z}}{2}\left(\frac{1}{\bar{z}-s} - \frac{1}{\bar{z}-\sigma}\right) - \frac{C}{2}\log\left(-\frac{\bar{z}-s}{s(\bar{z}-\sigma)}\right)\right]_{\mathcal{C}} \\ &= -2\mu C\,\Im\left[\log(\bar{z}-s) - \log(\bar{z}-\sigma)\right]_{\mathcal{C}}.\end{aligned} \tag{34}$$

To evaluate $\mathcal{M}$, we must now proceed with caution. If $|s| < a$, the original rotlet singularity at $z = s$ lies inside the contour $\mathcal{C}$ and $[\log(\bar{z}-s)]_{\mathcal{C}} = -2\mathrm{i}\pi$. The image singularity at $z = \sigma$ lies outside the boundary and so the term $\log(\bar{z}-\sigma)$ is unchanged by a tour of $\mathcal{C}$. By contrast, when the rotlet is placed outside the cylinder, with $|s| > a$, the situation is reversed and the *image* singularity makes an equal and opposite contribution to $\mathcal{M}$. Hence

$$\mathcal{F} = 0, \tag{35}$$

$$\mathcal{M} = \begin{cases} 4\pi\mu C & \text{if } |s| < a \\ -4\pi\mu C & \text{if } |s| > a. \end{cases} \tag{36}$$

3.3. THE ENERGETICS OF THE MODIFIED STOKESLET

The functions $F(z)$ and $G(z)$ corresponding to a modified stokeslet in the presence of a cylindrical boundary are found by adding together the respective expressions in (19), (20), (23) and (24), with P, Q and R given by (28). For the purpose of the energetics calculation we need to consider only the multivalued components of F and G:

$$F(z) = \tfrac{1}{4}(A + \mathrm{i}B)\log\left(-\frac{z-s}{s(z-\sigma)}\right), \tag{37}$$

$$G(z) = \tfrac{1}{4}(A - \mathrm{i}B)z\log\left(-\frac{z-s}{s(z-\sigma)}\right). \tag{38}$$

When these expressions are applied as in Section 3.1, taking $\mathcal{C}$ as the perimeter of the cylinder once again, we find that the force and moment exerted by the cylinder on the fluid are

$$\mathcal{F} = \begin{cases} 4\pi\mu(B - \mathrm{i}A) & \text{if } |s| < a \\ -4\pi\mu(B - \mathrm{i}A) & \text{if } |s| > a, \end{cases} \tag{39}$$

$$\mathcal{M} = 0. \tag{40}$$

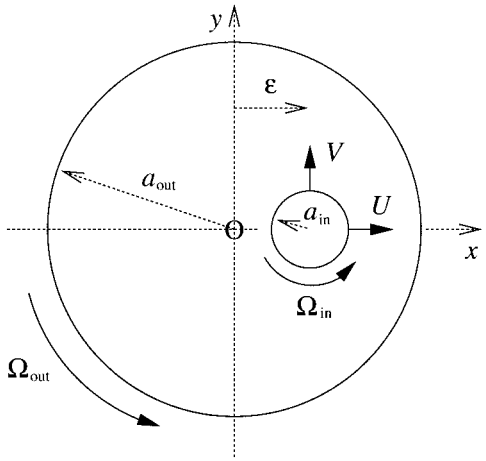

Figure 4. The geometry of the translating, rotating mixer. Fluid fills the annular region between the inner and outer cylinders (with radii a_{in} and a_{out}, respectively). These cylinders may each rotate about their own axes, with angular velocities Ω_{in} and Ω_{out}. In addition the inner cylinder may translate, with velocity (U, V). The origin of the Cartesian coordinate system coincides with the axis of the outer cylinder, and the axis of the inner cylinder is at $(\epsilon, 0)$, where ϵ is the eccentricity. At each instant the coordinate system is chosen so that the axis of the inner cylinder lies on the x-axis.

3.4. THE ENERGETICS OF GENERAL IMAGE SYSTEMS

For a streamfunction ψ of the form (4) whose image system is given by Ψ of the form (8), there are two useful relationships between the functions f, g, F and G that allow us to compute the forces and moments due to Ψ using the relatively simple functions f and g instead of the more complicated functions F and G. These relationships, readily confirmed from (9) and (10), are

$$\left[-F(z) + z\bar{F}'(\bar{z}) + \bar{G}'(\bar{z})\right]_{\mathcal{C}} = 2\left[-f(z) + z\bar{f}'(\bar{z}) + \bar{g}'(\bar{z})\right]_{\mathcal{C}}, \tag{41}$$

$$\left[z\bar{z}\bar{F}'(\bar{z}) + \bar{z}\bar{G}'(\bar{z}) - \bar{G}(\bar{z})\right]_{\mathcal{C}} = 2\left[z\bar{z}\bar{f}'(\bar{z}) + \bar{z}\bar{g}'(\bar{z}) - \bar{g}(\bar{z})\right]_{\mathcal{C}}. \tag{42}$$

In applications, it may be that one form results in an easier calculation than the other, although for the two examples above there is little difference in the computational effort required in using the different expressions.

4. The translating, rotating mixer

We are now in a position to describe the translating, rotating mixer, which is illustrated in Figure 4. The inner and outer boundaries of the fluid domain are the circles $|z - \epsilon| = a_{\text{in}}$ and $|z| = a_{\text{out}}$, respectively, where the (real) eccentricity ϵ is not necessarily small. The outer cylinder may rotate about its axis, with angular velocity Ω_{out}, and so the boundary condition to be satisfied there is

$$u + \mathrm{i}v = \mathrm{i}\Omega_{\text{out}} z \quad \text{at } |z| = a_{\text{out}}. \tag{43}$$

At the inner cylinder, in addition to a rotation of the boundary with angular velocity Ω_{in}, a translation velocity (U, V) is permitted, so the corresponding boundary condition is

$$u + \mathrm{i}v = U + \mathrm{i}V + \mathrm{i}\Omega_{\text{in}}(z - \epsilon) \quad \text{at } |z - \epsilon| = a_{\text{in}}. \tag{44}$$

Recall that we consider Stokes flow, at vanishingly small Reynolds number, so that the streamfunction ψ satisfies the biharmonic equation (1). Since this governing equation and the boundary conditions are linear in ψ, we may construct the streamfunction for the rather complicated general motion of the device by superposing solutions corresponding to individual components of the motion. These component solutions are given in the following subsections, and are assembled in Section 4.5 to give the complete streamfunction.

We note that our geometry is set up with the axis of the inner cylinder lying on the x-axis. Of course, if the y-component of its velocity is nonzero, then it will immediately move off this axis. However, rather than present below the streamfunction for the TRM with the inner cylinder in an arbitrary position, we instead choose to present the streamfunction for the 'canonical' geometry in Figure 4, noting that any other location of the inner cylinder may be obtained by a rotation of the coordinate axes.

4.1. Some geometrical considerations

In the following subsections, we shall construct the streamfunction for the translating, rotating mixer by applying the method of images to various singularities. As a precursor to this calculation, we note in this subsection some identities that will enable us to match the *locations* of the singularities with the geometrical parameters of the mixer. (The requisite *strengths* of the singularities will be the subject of the next few subsections.)

A rotlet or modified stokeslet at $z = s \in \mathfrak{R}$ (with image point $z = \sigma$, where $s\sigma = a_{\text{out}}^2$) generates images that result in a streamfunction containing the logarithm

$$L \equiv \log \frac{\sigma|z-s|^2}{s|z-\sigma|^2}.$$

To satisfy boundary conditions of the form contemplated above in (43) and (44), we need to ensure that this logarithm is constant on the inner and outer boundaries. By construction, on the outer boundary, where $|z| = a_{\text{out}}$, this logarithm automatically vanishes. On the inner boundary, where $|z-\epsilon| = a_{\text{in}}$, it can be made constant by choosing s so that

$$a_{\text{in}}^2 = (s-\epsilon)(\sigma-\epsilon), \tag{45}$$

in which case

$$L = \log \frac{\sigma(s-\epsilon)}{s(\sigma-\epsilon)}. \tag{46}$$

Given the geometrical parameters a_{in}, a_{out} and ϵ, the corresponding value of σ is then

$$\frac{a_{\text{out}}^2 - a_{\text{in}}^2 + \epsilon^2 + \{(a_{\text{out}}+a_{\text{in}}+\epsilon)(a_{\text{out}}+a_{\text{in}}-\epsilon)(a_{\text{out}}-a_{\text{in}}+\epsilon)(a_{\text{out}}-a_{\text{in}}-\epsilon)\}^{1/2}}{2\epsilon}, \tag{47}$$

with s being given by the expression above, but taking minus the square root.

In addition, once the relationship (45) is adopted, it follows after a little algebra that

$$-\frac{|z|^2 - a_{\text{out}}^2}{|z-\sigma|^2} = \frac{\epsilon}{\sigma-\epsilon}, \quad -\frac{|z|^2 - a_{\text{out}}^2}{|z-s|^2} = \frac{\epsilon}{s-\epsilon}. \tag{48}$$

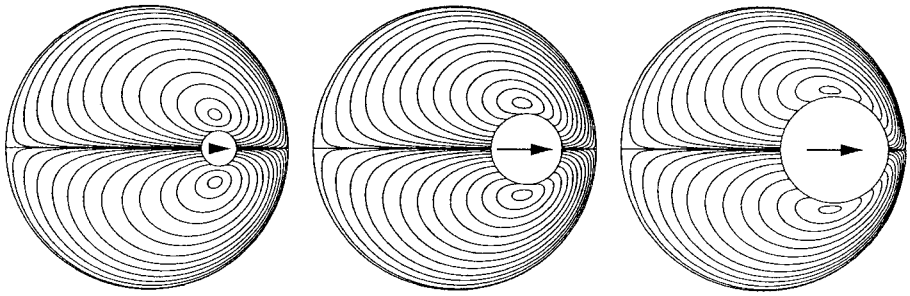

Figure 5. Streamline patterns corresponding to x-translation of the inner cylinder, with a fixed outer cylinder. In each picture the axis of the inner cylinder is instantaneously at the point $(\frac{1}{2}a_{\rm out}, 0)$. From left to right $a_{\rm in}/a_{\rm out} = 1/8, 2/8, 3/8$.

Finally, we note that, according to (45),

$$(z-\epsilon)(\bar{z}-\epsilon) = (s-\epsilon)(\sigma-\epsilon) \tag{49}$$

on the inner cylinder. This equation is useful for eliminating $\bar{z}$ in favour of z on $|z-\epsilon| = a_{\rm in}$.

4.2. x-TRANSLATION OF THE INNER CYLINDER

In this subsection, we derive the streamfunction that corresponds to motion of the inner cylinder along the real axis, with neither cylinder rotating, so that $V = 0$ and $\Omega_{\rm in} = \Omega_{\rm out} = 0$ in (43) and (44).

We consider a streamfunction in the form of a modified stokeslet of strength $\mathrm{i}B$ at $z = s$ and a modified stokeslet of strength $\mathrm{i}\beta$ at the image point $z = \sigma$, where $s\sigma = a_{\rm out}^2$. Then, according to (29),

$$\begin{aligned}\psi \;=\; & -\tfrac{1}{4}\mathrm{i}(B-\beta)(z-\bar{z})\log\frac{\sigma|z-s|^2}{s|z-\sigma|^2} \\ & + \tfrac{1}{4}\mathrm{i}(z-\bar{z})(\sigma-s)(|z|^2-a_{\rm out}^2)\left\{\frac{B}{s|z-\sigma|^2}-\frac{\beta}{\sigma|z-s|^2}\right\}.\end{aligned} \tag{50}$$

By the method of images described in Section 2, we are assured that the homogeneous boundary conditions at $|z| = a_{\rm out}$ are satisfied, and it remains to impose the condition $u + \mathrm{i}v = U$ at $|z-\epsilon| = a_{\rm in}$. To do so, we first calculate the velocity field using (5), which gives

$$\begin{aligned}u+\mathrm{i}v \;=\; & \tfrac{1}{2}(B-\beta)\log\frac{\sigma|z-s|^2}{s|z-\sigma|^2} - \tfrac{1}{2}(\sigma-s)\left\{\frac{B(|z|^2-a_{\rm out}^2)}{s|z-\sigma|^2}-\frac{\beta(|z|^2-a_{\rm out}^2)}{\sigma|z-s|^2}\right\} \\ & + \tfrac{1}{2}(\sigma-s)(z-\bar{z})\left\{-\frac{B(|z|^2-a_{\rm out}^2)}{s(z-\sigma)(\bar{z}-\sigma)^2}+\frac{\beta(|z|^2-a_{\rm out}^2)}{\sigma(z-s)(\bar{z}-s)^2}\right. \\ & \left. + z\frac{B}{s|z-\sigma|^2} - z\frac{\beta}{\sigma|z-s|^2} + \frac{B-\beta}{(\bar{z}-s)(\bar{z}-\sigma)}\right\}.\end{aligned} \tag{51}$$

The expression for the velocity on the inner boundary may be considerably simplified using the identities in (48) and (49) to give

$$\begin{aligned}u+\mathrm{i}v \;=\; & \tfrac{1}{2}(B-\beta)L + \tfrac{1}{2}(\sigma-s)\left\{\frac{B\epsilon}{s(\sigma-\epsilon)}-\frac{\beta\epsilon}{\sigma(s-\epsilon)}\right\} \\ & - \frac{(\sigma-s)(z-\bar{z})}{2(\bar{z}-s)(\bar{z}-\sigma)}\left\{\frac{\epsilon(\sigma-s)(\epsilon(B\sigma+\beta s)-(B+\beta)s\sigma)}{s\sigma(s-\epsilon)(\sigma-\epsilon)}\right\},\end{aligned} \tag{52}$$

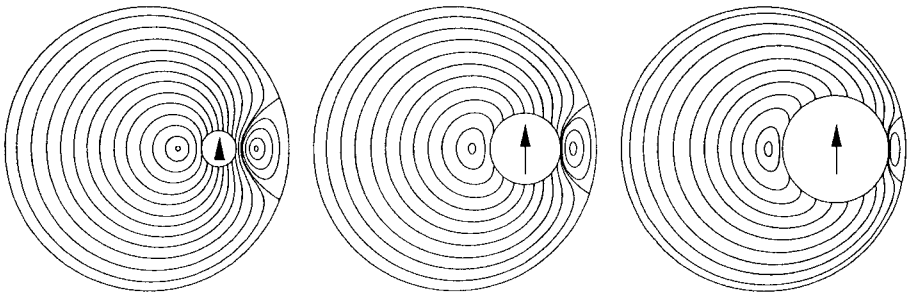

Figure 6. Streamline patterns for the y-translation of the inner cylinder, with a fixed outer cylinder. In each picture the axis of the inner cylinder is instantaneously at the point $(\frac{1}{2}a_{\rm out}, 0)$. From left to right $a_{\rm in}/a_{\rm out} = 1/8,\ 2/8,\ 3/8$.

where L is given by (46). We are now in a position to apply the boundary condition $u+{\rm i}v = U$ to (52), which requires

$$\epsilon(B\sigma + \beta s) - (B+\beta)s\sigma = 0, \tag{53}$$

$$\tfrac{1}{2}(B-\beta)L + \tfrac{1}{2}(\sigma - s)\left\{\frac{B\epsilon}{s(\sigma-\epsilon)} - \frac{\beta\epsilon}{\sigma(s-\epsilon)}\right\} = U. \tag{54}$$

From this pair of equations, we finally obtain the stokeslet strengths

$$B = \frac{2U(\sigma-\epsilon)s}{2\epsilon(\sigma-s) + (a_{\rm in}^2 + a_{\rm out}^2 - \epsilon^2)L}, \tag{55}$$

$$\beta = \frac{-2U(s-\epsilon)\sigma}{2\epsilon(\sigma-s) + (a_{\rm in}^2 + a_{\rm out}^2 - \epsilon^2)L}. \tag{56}$$

These expressions agree with those presented by Secomb and El-Kareh [21], after conversion to bipolar coordinates. Typical streamlines are illustrated in Figure 5.

4.3. y-TRANSLATION AND ROTATION OF THE INNER CYLINDER

In this subsection, we derive the streamfunction for motion of the inner cylinder comprising translation in the y-direction and rotation about its axis. We consider a modified stokeslet of strength A and rotlet of strength C at $z = s$. We also consider a modified stokeslet of strength α and a rotlet of strength γ at the image point $z = \sigma$. The streamfunction corresponding to these singularities, together with their images in the outer boundary, is, according to Sections 2.1 and 2.2,

$$\begin{aligned}\psi = {} & \left\{\tfrac{1}{4}(A-\alpha)(z+\bar z) + \tfrac{1}{2}(C-\gamma)\right\}\log\frac{\sigma|z-s|^2}{s|z-\sigma|^2} \\ & + (|z|^2 - a_{\rm out}^2)\left\{\frac{A}{4s}\left(\frac{z+s}{z-\sigma} + \frac{\bar z + s}{\bar z - \sigma}\right) + \frac{\alpha}{4\sigma}\left(\frac{z+\sigma}{z-s} + \frac{\bar z + \sigma}{\bar z - s}\right)\right. \\ & \left. + \frac{C(|z|^2-\sigma^2)}{2a_{\rm out}^2|z-\sigma|^2} + \frac{\gamma(|z|^2-s^2)}{2a_{\rm out}^2|z-s|^2}\right\}.\end{aligned} \tag{57}$$

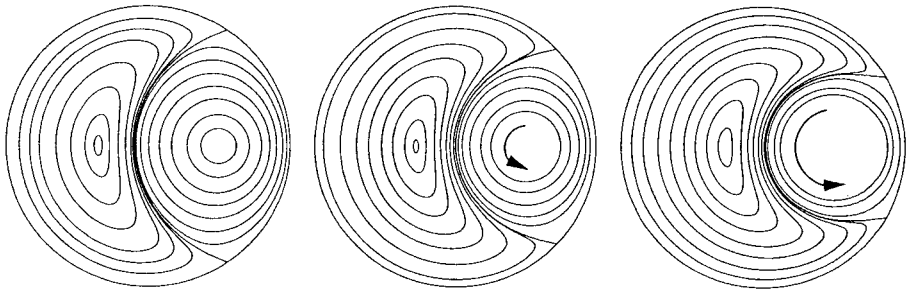

Figure 7. Streamline patterns corresponding to rotation of the inner cylinder, with a fixed outer cylinder. In each picture the axis of the inner cylinder is at the point $(\frac{1}{2}a_{\rm out}, 0)$. From left to right $a_{\rm in}/a_{\rm out} = 1/8,\ 2/8,\ 3/8$.

This streamfunction gives rise, through (5), to the velocity field

$$\begin{aligned} u + \mathrm{i}v \;=\; & \tfrac{1}{2}\mathrm{i}(A-\alpha)\left\{\frac{(z+\bar z)(\sigma-s)}{(\bar z-s)(\bar z-\sigma)} - \log\frac{\sigma|z-s|^2}{s|z-\sigma|^2}\right\} \\ & + \tfrac{1}{2}\mathrm{i}A\left\{\frac{(|z|^2-a_{\rm out}^2)(\sigma+s)}{(\bar z-\sigma)^2 s} - \frac{z}{s}\left(\frac{z+s}{z-\sigma}+\frac{\bar z+s}{\bar z-\sigma}\right)\right\} \\ & + \tfrac{1}{2}\mathrm{i}\alpha\left\{\frac{(|z|^2-a_{\rm out}^2)(\sigma+s)}{(\bar z-s)^2\sigma} - \frac{z}{\sigma}\left(\frac{z+\sigma}{z-s}+\frac{\bar z+\sigma}{\bar z-s}\right)\right\} \\ & - \mathrm{i}C\left\{\frac{z^2}{a_{\rm out}^2(z-\sigma)} - \frac{z\sigma-a_{\rm out}^2}{s(\bar z-\sigma)^2} - \frac{1}{\bar z-\sigma} + \frac{1}{\bar z-s}\right\} \\ & - \mathrm{i}\gamma\left\{\frac{z^2}{a_{\rm out}^2(z-s)} - \frac{zs-a_{\rm out}^2}{\sigma(\bar z-s)^2} - \frac{1}{\bar z-s} + \frac{1}{\bar z-\sigma}\right\}. \end{aligned} \tag{58}$$

By construction, the boundary condition (43) is automatically satisfied, with $\Omega_{\rm out} = 0$. To satisfy the boundary condition (44) with $U = 0$, we equate the right-hand side of (58) to $\mathrm{i}V + \mathrm{i}\Omega_{\rm in}(z-\epsilon)$ on the inner cylinder. It turns out after much algebra (relegated to a computer package) that the resulting equation simplifies to

$$K_0 + K_1 z + K_2 z^2 + K_3 z^3 \equiv 0, \tag{59}$$

where the four constants K_i are complicated expressions, but which depend only upon the geometry of the mixer, and upon V and $\Omega_{\rm in}$. The condition (59) is satisfied by setting each of the K_i to zero, resulting in four linear equations for A, α, C and γ. However, these equations are not linearly independent, and we are free to impose one further condition: a symmetry in the coefficients A, α, C and γ is obtained by specifying $C = -\gamma$, which gives

$$A \;=\; s\epsilon\frac{a_{\rm in}^2(2\epsilon - L\sigma)\Omega_{\rm in} - 2V(\sigma^2+a_{\rm in}^2)}{(a_{\rm out}^2 - a_{\rm in}^2 + \epsilon^2)\{2(\sigma-s)\epsilon + (a_{\rm in}^2+a_{\rm out}^2)L\}}, \tag{60}$$

$$\alpha \;=\; -\sigma\epsilon\frac{a_{\rm in}^2(2\epsilon + Ls)\Omega_{\rm in} - 2V(s^2+a_{\rm in}^2)}{(a_{\rm out}^2 - a_{\rm in}^2 + \epsilon^2)\{2(\sigma-s)\epsilon + (a_{\rm in}^2+a_{\rm out}^2)L\}}, \tag{61}$$

$$C \;=\; -a_{\rm out}^2\frac{a_{\rm in}^2(2(\sigma-s)\epsilon + (a_{\rm in}^2+a_{\rm out}^2-\epsilon^2)L)\Omega_{\rm in} - 2V\epsilon^2(\sigma-s)}{2\epsilon(\sigma-s)\{2(\sigma-s)\epsilon + (a_{\rm in}^2+a_{\rm out}^2)L\}}, \tag{62}$$

$$\gamma \;=\; a_{\rm out}^2\frac{a_{\rm in}^2(2(\sigma-s)\epsilon + (a_{\rm in}^2+a_{\rm out}^2-\epsilon^2)L)\Omega_{\rm in} - 2V\epsilon^2(\sigma-s)}{2\epsilon(\sigma-s)\{2(\sigma-s)\epsilon + (a_{\rm in}^2+a_{\rm out}^2)L\}}. \tag{63}$$

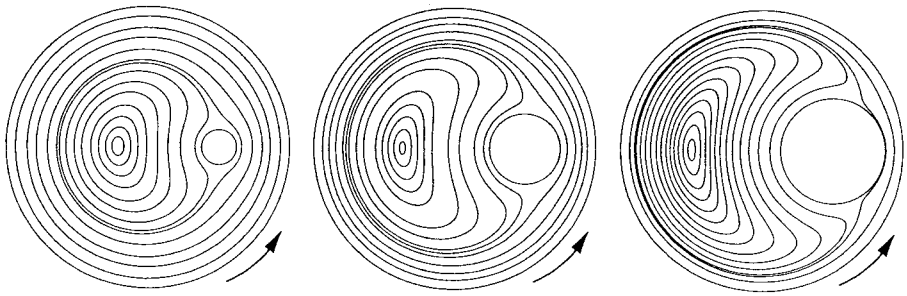

Figure 8. Streamline patterns corresponding to rotation of the outer cylinder, with a fixed inner cylinder. In each picture the axis of the inner cylinder is at the point $(\frac{1}{2}a_{\text{out}}, 0)$. From left to right $a_{\text{in}}/a_{\text{out}} = 1/8,\ 2/8,\ 3/8$.

Typical streamlines for y-translation and for rotation of the inner cylinder are shown in Figures 6 and 7.

4.4. Rotation of the outer cylinder

By construction, the solutions (50) and (57) so far each satisfy $u + \mathrm{i}v = 0$ on the outer boundary. To see how to accommodate a rotation of the outer boundary, we consider the influence of the streamfunction

$$\psi = -\tfrac{1}{2}\Omega_{\text{out}}(|z|^2 - a_{\text{out}}^2). \tag{64}$$

At the outer cylinder, this clearly corresponds to a rotation with angular velocity Ω_{out}. At the inner cylinder, it gives the velocity field $u + \mathrm{i}v = \mathrm{i}\Omega_{\text{out}}z$, which may be separated into the two components

$$u + \mathrm{i}v = \mathrm{i}\epsilon\Omega_{\text{out}} + \mathrm{i}\Omega_{\text{out}}(z - \epsilon), \tag{65}$$

and these can in turn be identified, respectively, as a y-translation of the inner cylinder with speed $\epsilon\Omega_{\text{out}}$ and a rotation about its axis with angular velocity Ω_{out}. These extraneous motions of the inner cylinder can be removed by noting the identity

$$\psi(z, \bar{z}; U, V, \Omega_{\text{in}}, \Omega_{\text{out}}) = \psi(z, \bar{z}; U, V - \epsilon\Omega_{\text{out}}, \Omega_{\text{in}} - \Omega_{\text{out}}, 0) - \tfrac{1}{2}\Omega_{\text{out}}(|z|^2 - a_{\text{out}}^2), \tag{66}$$

i.e., by making the substitutions

$$\Omega_{\text{in}} \mapsto \Omega_{\text{in}} - \Omega_{\text{out}}, \quad V \mapsto V - \epsilon\Omega_{\text{out}} \tag{67}$$

in the coefficients (60)–(63). Typical streamlines due to the rotation of the outer cylinder, with a stationary inner cylinder, are shown in Figure 8.

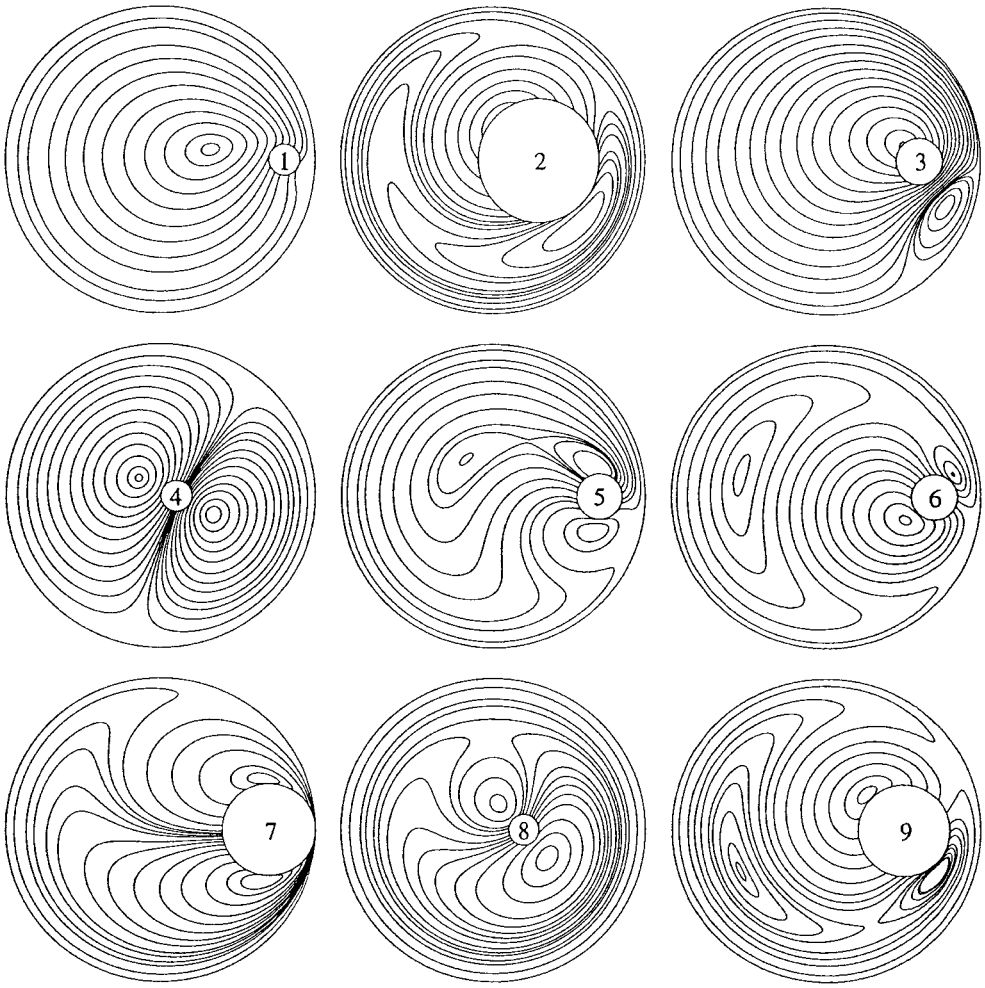

Figure 9. Some sample streamline patterns for the TRM, generated from (68) or (69). The parameter values for each image are given in Table 1. We have not undertaken a systematic cataloguing of the great variety of possible streamline patterns.

4.5. Overall solution

The final streamfunction, which allows for rotation of both cylinders about their axes and translation of the inner cylinder, is

$$\begin{aligned}\psi \;=\; & \left\{\tfrac{1}{4}(A-\alpha)(z+\bar{z}) - \tfrac{1}{4}\mathrm{i}(B-\beta)(z-\bar{z}) + \tfrac{1}{2}(C-\gamma)\right\}\log\frac{\sigma|z-s|^2}{s|z-\sigma|^2} \\ & + \tfrac{1}{2}(|z|^2 - a_{\mathrm{out}}^2)\left\{\frac{A}{2s}\left(\frac{z+s}{z-\sigma}+\frac{\bar{z}+s}{\bar{z}-\sigma}\right) + \frac{\alpha}{2\sigma}\left(\frac{z+\sigma}{z-s}+\frac{\bar{z}+\sigma}{\bar{z}-s}\right)\right. \\ & + \frac{\mathrm{i}B(z-\bar{z})(\sigma-s)}{2s|z-\sigma|^2} - \frac{\mathrm{i}\beta(z-\bar{z})(\sigma-s)}{2\sigma|z-s|^2} \\ & \left. + \frac{C(|z|^2-\sigma^2)}{a_{\mathrm{out}}^2|z-\sigma|^2} + \frac{\gamma(|z|^2-s^2)}{a_{\mathrm{out}}^2|z-s|^2} - \Omega_{\mathrm{out}}\right\}, \end{aligned} \tag{68}$$

Table 1. Parameter values corresponding to the images in Figure 9.

	1	2	3	4	5	6	7	8	9
$a_{\text{in}}/a_{\text{out}}$	0·1	0·4	0·15	0·1	0·15	0·15	0·3	0·1	0·3
ϵ/a_{out}	0·8	0·3	0·6	0·1	0·7	0·7	0·7	0·2	0·5
V/U	2	1	1	2	0	−1	0	1	1
$\Omega_{\text{in}}a_{\text{out}}/U$	−3	5	10	0	3·33	0	0	5	2
$\Omega_{\text{out}}a_{\text{out}}/U$	1	−3	0	0	0·66	0·66	−0·2	−1	−2

where the coefficients B and β are given by (55) and (56). The coefficients A, α, C and γ are given by (60)–(63) for $\Omega_{\text{out}} = 0$; their values for $\Omega_{\text{out}} \neq 0$ are determined similarly, but with the substitutions in (67). This streamfunction can be written in Cartesian coordinates, ready for numerical work, as

$$\begin{aligned}\psi \;=\; & \tfrac{1}{2}\{(A-\alpha)x + (B-\beta)y + (C-\gamma)\}\log\left\{\frac{\sigma}{s}\frac{(x-s)^2+y^2}{(x-\sigma)^2+y^2}\right\} \\ & + \tfrac{1}{2}(r^2 - a_{\text{out}}^2)\left\{\frac{A\{r^2 - a_{\text{out}}^2 - (\sigma-s)x\}/s - B(\sigma-s)y/s + C(r^2-\sigma^2)/a_{\text{out}}^2}{(x-\sigma)^2+y^2}\right. \\ & \left. + \frac{\alpha\{r^2 - a_{\text{out}}^2 + (\sigma-s)x\}/\sigma + \beta(\sigma-s)y/\sigma + \gamma(r^2-s^2)/a_{\text{out}}^2}{(x-s)^2+y^2} - \Omega_{\text{out}}\right\}, \qquad (69)\end{aligned}$$

where $r^2 = x^2 + y^2$. The corresponding streamlines can be quite complicated – a sample of the possibilities is shown in Figure 9. However, a full delineation in parameter space of all the topologically distinct flows is beyond the scope of this article.

4.6. The energetics of the TRM

We shall later compute the energy requirements of various stirring protocols used in numerical simulations of the TRM. In preparation for that calculation, we consider in this subsection the energetics of the TRM. Wannier [18] has computed the forces and moments acting on the boundaries in the case where they each rotate about their respective axes, and the inner cylinder does not translate; however, the details of his calculation were not presented. In the special case in which the radius of the outer cylinder becomes infinite, the corresponding forces and moments have been calculated by Jeffrey and Onishi [25], and we have used their results to check ours in that limit.

We begin by noting that the TRM streamfunction is just a combination of rotlet and stokeslet singularities, together with their images: inside the outer cylinder, at $z = s$, are a modified stokeslet of strength $A + \mathrm{i}B$ and a rotlet of strength C; outside the cylinder, at $z = \sigma$, are a stokeslet of strength $\alpha + \mathrm{i}\beta$ and a rotlet of strength γ. By linearity, the force $\mathcal{F}_{\text{out}}$ and moment $\mathcal{M}_{\text{out}}$ about the origin exerted *by* the outer cylinder *on* the fluid is found by adding together the results (35), (36), (39) and (40) that apply to each individual rotlet and stokeslet. We find that the final expressions are

$$\mathcal{F}_{\text{out}} \;=\; 4\pi\mu(B - \beta - \mathrm{i}A + \mathrm{i}\alpha), \qquad (70)$$

$$\mathcal{M}_{\text{out}} \;=\; 4\pi\mu(C - \gamma). \qquad (71)$$

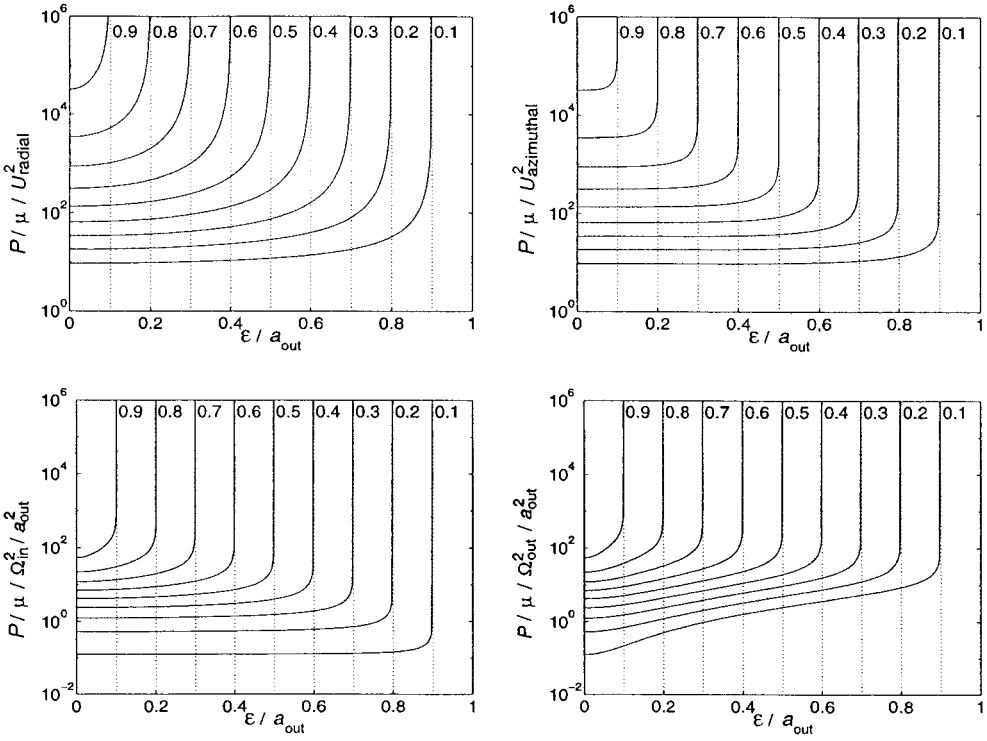

Figure 10. Power inputs required for radial translation with speed U_{radial} (top left), azimuthal translation with speed $U_{\text{azimuthal}}$ (top right), inner cylinder rotation (bottom left) and outer cylinder rotation (bottom right) in the TRM, where the power $\mathcal{P}$ is given by (75). The distance of the inner cylinder axis from the origin is ϵ, and each curve is marked with the corresponding value of $a_{\text{in}}/a_{\text{out}}$.

Since the mixing device is in overall equilibrium (or by repeating the analysis of Section 3 using the inner cylinder as the contour $\mathcal{C}$), we find that the force $\mathcal{F}_{\text{in}}$ and moment $\mathcal{M}$ about the origin exerted *by* the inner cylinder *on* the fluid are

$$\mathcal{F}_{\text{in}} = 4\pi\mu(\beta - B - \mathrm{i}\alpha + \mathrm{i}A), \tag{72}$$

$$\mathcal{M} = 4\pi\mu(\gamma - C). \tag{73}$$

In calculating the power input to the device, it is more useful to know instead the moment about the axis of the inner cylinder, which is thus

$$\mathcal{M}_{\text{in}} = \mathcal{M} - \epsilon\,\Im\,\mathcal{F}_{\text{in}} = 4\pi\mu(\gamma - C - \epsilon A + \epsilon\alpha). \tag{74}$$

The power input, per unit axial length of the device, is then

$$\begin{aligned}\mathcal{P} &\equiv (\Re\,\mathcal{F}_{\text{in}}, \Im\,\mathcal{F}_{\text{in}}) \cdot (U, V) + \mathcal{M}_{\text{in}}\Omega_{\text{in}} + \mathcal{M}_{\text{out}}\Omega_{\text{out}} \\ &= 4\pi\mu\left\{(\beta - B)U + (A - \alpha)V + (\gamma - C - \epsilon A + \epsilon\alpha)\Omega_{\text{in}} + (C - \gamma)\Omega_{\text{out}}\right\}. \end{aligned} \tag{75}$$

It is instructive to examine how the power input to the TRM required to maintain the various translational and rotational motions depends upon the position of the inner cylinder. Figure 10 shows the variation with eccentricity of the power inputs required for the four different motions (radial and azimuthal translation of the inner cylinder, and rotation of the inner and outer cylinders). As one would expect, the power requirements for radial and azimuthal

Table 2. Three different cycloid stirring protocols used in our experiments. The parameters r_1, r_2 and n correspond to the cycloid path given in (76), and λ is the length of this path.

Protocol	r_1/a_{out}	r_2/a_{out}	n	λ/a_{out}
−4:1	0·42	0·31	−4	8·02
+4:1	0·21	0·53	+4	13·35
+6:1	0·31	0·42	+6	15·89

translation coincide as $\epsilon \to 0$ since the distinction between different directions of motion is lost when the cylinders are concentric. With the scalings adopted in Figure 10, the power requirements for rotation of the inner and outer cylinders also coincide as $\epsilon \to 0$. We note from Figure 10 that the power needed to rotate the outer cylinder increases much more rapidly as a function of eccentricity than does that for the inner cylinder. As the two cylinders approach one other, *i.e.*, as $\epsilon \to a_{\text{out}} - a_{\text{in}}$, all the power inputs diverge (*cf.* [18, 25]). When the cylinders are close, but not touching, more power is required to move the inner cylinder perpendicular to the wall than parallel to it [25].

5. Numerical and experimental results

Having established the velocity field for the TRM, we now describe a selection of numerical stirring simulations and experiments with the device. We present below comparisons between our numerical and experimental results; these serve in part as a validation of the various modelling assumptions that we have made, in particular that the flow is quasi-steady and sufficiently slow that it is governed by (1), and that the flow is well approximated as two-dimensional. The experiments provide encouraging agreement with the numerical simulations.

Our method of stirring involves translating a rod (the inner cylinder) of circular cross-section and relatively small radius so that its axis moves along a prescribed path $(x, y) = (X(t), Y(t))$ inside the fixed outer cylinder, where the parameter t is time. We have chosen each path to be a cycloid of the form

$$(X, Y) = (r_1 \cos(2\pi t/T) + r_2 \cos(2\pi n t/T), r_1 \sin(2\pi t/T) + r_2 \sin(2\pi n t/T)); \qquad (76)$$

the parameters r_1, r_2 and n determine the exact shape of the cycloid. We consider integer values for n and as a consequence the cycloid stirring period is T.

The choice of a cycloid as the stirring path was motivated by the comparative ease with which such a path can be generated experimentally using straightforward gearing. Although many, more complicated stirring protocols can be envisaged, for example, involving rotation of one or both cylinders during some part of the cycle, we were unable to reproduce these more complicated protocols with our modest experimental set-up. Furthermore, we have found in numerical simulations that the use of more complicated stirring protocols usually requires increased power input, but does not necessarily improve stirring quality. With a more sophisticated experimental facility, it may of course be possible to implement rotation of the inner or outer cylinders; such motions are readily accommodated in (69).

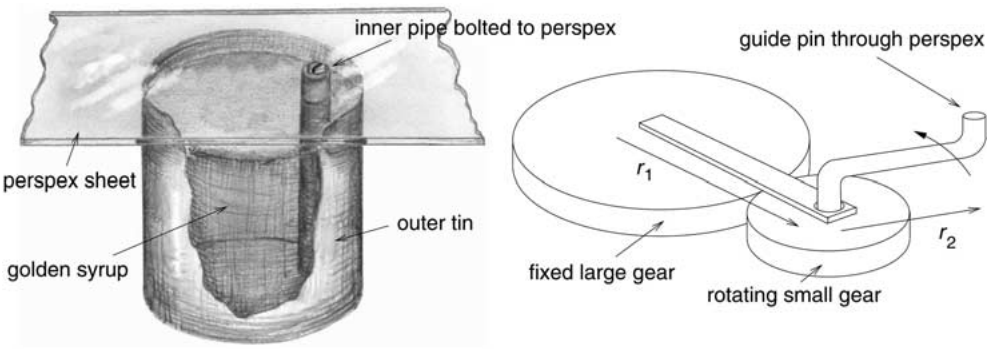

Figure 11. The experimental TRM. On each side of the vat of fluid is an identical arrangement of arms and gears (one set is shown here). The larger gear wheel is fixed to the bench and the smaller gear wheel rotates around it. An S-shaped arm is fixed at one end to the smaller gear wheel; the other end, which traces out a cycloid as the smaller gear wheel rotates, passes through a hole in the perspex sheet to guide its motion and thus the motion of the inner cylinder.

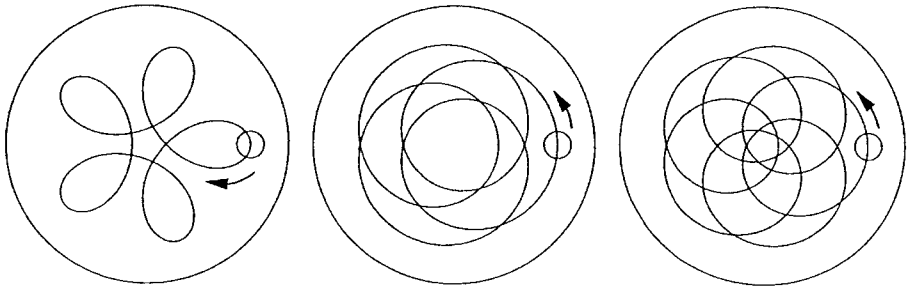

Figure 12. The cycloids followed by the inner cylinder in our experiments. From left to right are shown the −4:1, +4:1 and +6:1 protocols, named according to Table 2.

Our experimental apparatus consisted of a large coffee tin ($a_{\text{out}} = 7{\cdot}8$ cm) for an outer cylinder and a length of copper pipe ($a_{\text{in}} = 0{\cdot}75$ cm) for an inner cylinder. The pipe was bolted to a sheet of perspex which rested across the rim of the coffee tin. This perspex sheet was then guided on both sides by a simple arrangement of arms and gears which traced out the cycloid, and hence led the copper pipe to follow the same path (see Figure 11). Different cycloids were obtained by changing the lengths of the arms and by using different numbers of teeth on the gears. The guiding mechanisms were placed out of view of the top of the outer cylinder to permit photographs to be taken of the mixer. With the gears we had at our disposal we could reproduce the three stirring protocols in Table 2 – the total length $\lambda = \oint (U^2 + V^2)^{1/2}\,\mathrm{d}t$ of each complete cycloid is shown in this table, and the path shapes are illustrated in Figure 12. Although the viscosity of the fluid (golden syrup) is highly variable as a function of temperature, we estimate the Reynolds number of the flows we have generated to be $O(10^{-3})$ or smaller (where we have used as a length scale a_{out}, as a velocity scale a_{out}/T, where $T \approx 120$ s is the period of the cycloid, and where we have taken the kinematic viscosity of golden syrup to be approximately 1000 cm^2 s^{-1} – see [41], p. 28).

The coffee tin was filled with golden syrup and we then followed the mixing of a small blob of 'tracer' as the stirring action was played out. We used acrylic paint in golden syrup as tracer, floated on the surface so that it was visible to a digital camera overhead. Of course, such a procedure introduces the prospect of surface effects that are a potential source of discrepancy

Figure 13. Comparison between numerical simulations (top row) and experiments (bottom row) using the -4:1 stirring protocol. The leftmost images show the initial (nominally) circular blob of radius $0.14a_{\text{out}}$ centred at the point $(x, y) = (0.20, 0.30)a_{\text{out}}$. The following snapshots show the blob after one, two and three complete stirring cycles.

Figure 14. Further comparisons between numerical and experimental results. A circular blob of radius $0.14a_{\text{out}}$ placed at the centre of the outer cylinder was stirred for three cycles. The left-hand pair of images shows the results using the $+4$:1 protocol (numerical then experimental); the right-hand pair corresponds likewise to the $+6$:1 protocol.

between the experiments and numerical simulations. Furthermore, with the concentration of paint used, there remains the likelihood of significant viscosity differences (or, worse, of different rheology) between the (supposedly passive) tracer and the bulk fluid. However, the actual discrepancies turn out to be small, as the results that follow demonstrate.

To simulate numerically the evolution of a blob of tracer under the stirring action, we considered the blob to be made up of a large number of fluid particles, then integrated the positions of these particles forwards in time using the streamfunction (69). Figures 13 and 14 show the agreement between the numerical simulations and the experimental runs. The numerical simulations generally capture very well the broad features of the corresponding experimental runs, and also many of the finest structures of the flow. Although not all of the fine details of the stretched blob are reproduced by the numerical simulation, the agreement is remarkably good, given our experimental apparatus.

It is evident in both the numerics and experiments that each protocol provides a different mixing quality, and it remains to attempt to quantify this distinction. One typical diagnostic tool for assessing the mixing quality is the rate of stretching of the blob perimeter that is achieved by the mixing. We found that these stretching rates were least with the -4:1 protocol

Figure 15. Iterated mappings, computed numerically, for the stirring protocols used in our experiments. From left to right the images correspond to the -4:1, $+4$:1 and $+6$:1 stirring protocols.

and greatest with the $+6$:1 protocol, although the length stretch was so great with all protocols that we were unable properly to resolve the entire boundary after even moderate times.

The ability to generate high interface stretch rates is not the only important indicator of the quality of a mixing device: uniformity of mixing over the entire flow domain is also important in applications. To illustrate this, we show in Figure 15 iterated mappings for each stirring protocol, generated by following approximately thirty fluid particles and superimposing their locations after each period of the device (*i.e.*, at $t = mT$ for integers m up to several thousand). These iterated mappings reveal periodic islands where mixing quality is poor for each of the three stirring protocols. It is the simplest protocol (-4:1) that has the smallest area of visible islands and which therefore appears to offer the most uniform mixing. There are two large islands for the $+6$:1 protocol, which occupy almost half the stirring domain; we conclude that the mixing is correspondingly poor (uneven).

When evaluating the different stirring protocols, account should be taken not only of the final effect of the mixing on the blob, but also of the energy input required to achieve the mixing. Figure 16 shows, using the results of Section 4.6, the power and energy input required to drive each of the three stirring protocols. Our comparisons are based on requiring each mixer to complete its cycloid stirring protocol in a time T, as in (76). (This period is significant because in slow flow the energy required to carry out a given number of mixing cycles can be reduced by a factor of k merely by running the mixer k times as slowly.) The cycloid corresponding to the -4:1 protocol is by far the shortest and consequently is traversed the most slowly; this protocol demands, in each cycle, less than half the energy of the $+4$:1 protocol, and less than one-third that of the $+6$:1 protocol.

With the three protocols that we have investigated, we find that increasing the length of the cycloid leads to a greater stretching of the blob interface per cycle, but at the cost of a greater energy input and less uniform mixing. However, it would be unwise to attempt to extrapolate from these results to a more general case as it seems unlikely that *greater* stretching of the blob interface is generally associated with *less* uniform mixing. There is clearly much scope for further numerical and experimental investigation: given the rich variety of streamline patterns possible in the TRM (see Figure 9), the present results are far from being exhaustive.

6. Conclusion

The mixer that we have described mimics a natural mixing technique for a range of mixing problems, whose every-day manifestations include stirring (newtonian) paint with a length of dowel or stirring a mug of coffee (albeit with a spoon of circular cross-section). The mixing

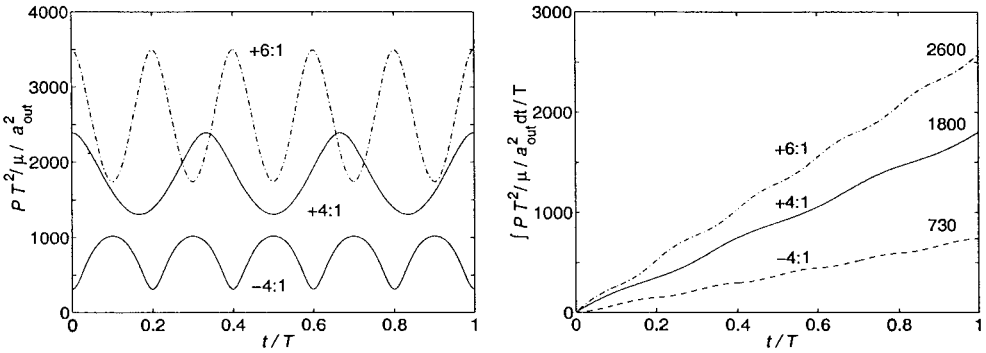

Figure 16. The left-hand plot shows the dimensionless power ($\mathcal{P}T^2/\mu/a_{\text{out}}^2$) required to drive the three experimental stirring protocols when the inner cylinder is moved according to (76), with the outer cylinder fixed (stirring protocol is indicated on each curve). The right-hand plot shows the dimensionless energy ($\int_0^t \mathcal{P}(t')T^2/\mu/a_{\text{out}}^2\,\mathrm{d}t'/T$) expended in stirring the device through one complete cycle (stirring protocol and total dimensionless energy expenditure are indicated on each curve).

takes place in laminar flow, which is appropriate in an industrial context for delicate long-chain polymers and bio-molecules. The mixer has a time-dependent geometry, which is the case for any mixer designed with moving parts, but despite this complication its velocity field can be computed exactly in closed form, by means of the slow-flow, quasi-static approximation. The changing geometry of the mixing device allows more effective stirring protocols than is possible in mixers with a fixed geometry, essentially because the inner cylinder can regularly plough through otherwise nearly 'dead' regions of the flow (such as arise commonly in the eccentric annular mixer, for example). This improvement in the mixing is in accord with the common-sense notion that to stir effectively, you move your stirring implement through the fluid rather than just turn it at a fixed location.

We have found that our mixer is readily constructed (for example, for demonstration purposes). Furthermore, the many assumptions made in deriving the exact velocity field (that there is slow, two-dimensional, quasi-steady flow) do not preclude good agreement between numerical simulation and experiment. It would be interesting for future studies in more sophisticated experimental facilities to investigate whether it is true for more general paths than cycloids that increasing the length of the path traced out by the inner cylinder in one cycle leads to greater stretching of the blob interface at the expense of greater energy input and less uniform mixing.

It is clear from the sample of streamline patterns in Figure 9 that by combining the various rotational and translation motions of the mixer boundaries, a wide range of flows is possible, with complicated, asymmetrical streamline patterns containing elliptic and hyperbolic points. We have not attempted a systematic classification of the possible streamline patterns, nor of their bifurcations, although such a programme should be feasible and may suggest other effective stirring protocols. In particular, we have not given numerical or experimental results for a rotating inner or outer cylinder, because we have been unable to achieve these motions with our experimental rig. However, it would be of interest to investigate whether mixing might be improved by implementing a rotation of one or other boundary cylinder.

The TRM generates excellent mixing, and it does so in slow laminar flow, which tends to avoid the extreme shear rates present in turbulent flow. While this feature of the device suggests that it might be useful for the bioprocess industry, it suffers a number of shortcom-

ings that might make it unsuitable for practical application in that area. Firstly, the mixing is two-dimensional, so that there is no axial motion of the fluid and hence no axial mixing, which can be important, for example in keeping cells suspended homogeneously. Also the smooth cylindrical nature of the stirring rod would make it unsuitable in a bioprocess such as fermentation, where a bladed impeller is useful in dispersing the fermentation gases [42, 43].

Acknowledgements

We are grateful to Christopher P. Finn for his assistance in producing the experimental photographs, and to Arthur England for discussions on the solution to the biharmonic equation in an annular region. This work has been supported by funding from the Division of Theoretical Mechanics in the School of Mathematical Sciences at the University of Nottingham.

References

1. V.V. Meleshko, O.S. Galaktionov, G.W.M. Peters and H.E.H. Meijer, Three-dimensional mixing in Stokes flow: the partitioned pipe mixer problem revisited. *Eur. J. Mech.* B/Fluids 18 (1999) 783–792.
2. C.R. Thomas, Problems of shear in biotechnology. In: M.A. Winkler (ed.), *Chemical Engineering Problems in Biotechnology*. Critical Reports on Applied Chemistry (1990) Vol. 29, pp. 23–93.
3. H. Aref, Stirring by chaotic advection. *J. Fluid Mech.* 143 (1984) 1–21.
4. J.M. Ottino, *The kinematics of mixing: stretching, chaos, and transport*. Cambridge Texts in Applied Mathematics. Cambridge University Press (1989) 364 pp.
5. S.C. Jana, M. Tjanjadi and J.M. Ottino, Chaotic mixing of viscous fluids by periodic changes in geometry: baffled cavity flow. *AIChE J.* 40 (1994) 1769–1781.
6. V.V. Meleshko and H. Aref, A blinking rotlet model for chaotic advection. *Phys. Fluids* 8 (1996) 3215–3217. (Errata in *Phys. Fluids* 10 (1998) 1543.)
7. H. Aref and S. Balachandar, Chaotic advection in a Stokes flow. Phys. Fluids 29 (1986) 3515–3521.
8. H. Aref and S.W. Jones, Enhanced separation of diffusing particles by chaotic advection. *Phys. Fluids A* 1 (1989) 470–474.
9. T. Atobe and M. Funakoshi, Chaotic motion of fluid particles due to the alternate rotations of two eccentric cylinders. *J. Phys. Soc. Japan* 63 (1994) 1738–1753.
10. T. Atobe, M. Funakoshi and S. Inoue, Orbital instability and chaos in the Stokes flow between two eccentric cylinders. *Fluid Dyn. Res.* 16 (1995) 115–129.
11. B.Y. Ballal and R.S. Rivlin, Flow of a Newtonian fluid between eccentric rotating cylinders: inertial effects. *Arch. Rat. Mech. Anal.* 62 (1976) 237–294.
12. J. Chaiken, R. Chevray, M. Tabor and Q.M. Tan, Experimental study of Lagrangian turbulence in a Stokes flow. *Proc. R. Soc. Lond. A* 408 (1986) 165–174.
13. J. Chaiken, C.K. Chu, M. Tabor and Q.M. Tan, Lagrangian turbulence and spatial complexity in a Stokes flow. *Phys. Fluids* 30 (1987) 687–694.
14. G.B. Jeffery, The rotation of two circular cylinders in a viscous fluid. *Proc. R. Soc. Lond.* A101 (1922) 169–174.
15. J.Y. Kazakia and R.S. Rivlin, Flow of a Newtonian fluid between eccentric rotating cylinders and related problems. *Stud. Appl. Math.* 58 (1978) 209–247.
16. W.E. Langlois, *Slow viscous flow*. New York: MacMillan (1964) 229 pp.
17. C. Pozrikidis, *Little book of streamlines*. Academic Press (1999) 148 pp.
18. G.H. Wannier, A contribution to the hydrodynamics of lubrication. *Q. Appl. Math.* 8 (1950) 1–32.
19. A.T. Chwang and T.Y.-T. Wu, Hydromechanics of low-Reynolds-number flow. Part 2. Singularity method for Stokes flows. *J. Fluid Mech.* 67 (1975) 787–815.
20. R.A. Frazer, On the motion of circular cylinders in a viscous fluid. *Phil. Trans. R. Soc. Lond.* A 225 (1926) 93–130.
21. T.W. Secomb and A.W. El-Kareh, A model for motion and sedimentation of cylindrical red-cell aggregates during slow blood flow in narrow horizontal tubes. *J. Biomech. Eng.* 116 (1994) 243–249.

22. A.C. Stevenson, Complex potentials in two-dimensional elasticity. *Proc. R. Soc. Lond.* A184 (1945) 129–179.
23. G.B. Jeffery, Plane stress and plane strain in bipolar coordinates. *Phil. Trans. R. Soc. Lond.* A221 (1921) 265–293.
24. L.M. Milne-Thomson, *Plane elastic systems*. Berlin: Springer–Verlag (1968) 211 pp.
25. D.J. Jeffrey and Y. Onishi, The slow motion of a cylinder next to a plane wall. *Q. Jl. Mech. Appl. Math.* 34 (1981) 129–137.
26. J.F. Trahan and R.G. Hussey, The Stokes drag on a horizontal cylinder falling toward a horizontal plane. *Phys. Fluids* 28 (1985) 2961–2969.
27. L.M. Milne-Thomson, *Theoretical hydrodynamics*. New York: Macmillan and Co. (1968).
28. H. Hasimoto and O. Sano, Stokeslets and eddies in creeping flow. *Ann. Rev. Fluid Mech.* 12 (1980) 335–363.
29. H.A. Lorentz, Eene algemeene stelling omtrent de beweging eener vloeistof met wrijving en eenige daaruit afgeleide gevolgen. *Zittingsverslag van de Koninklijke Akademie van Wetenschappen te Amsterdam* 5 (1896) 168–175. Translated into English by H.K. Kuiken, A general theorem on the motion of a fluid with friction and a few results derived from it. *J. Eng. Math.* 30 (1996) 19–24.
30. J.R. Blake, A note on the image system for a stokeslet in a no-slip boundary. *Proc. Camb. Phil. Soc.* 70 (1971) 303–310.
31. J.R. Blake and A.T. Chwang, Fundamental singularities of viscous flow. Part I: the image systems in the vicinity of a stationary no-slip boundary. *J. Eng. Math.* 8 (1974) 23–29.
32. J.R. Blake and S.R. Otto, Ciliary propulsion, chaotic filtration and a 'blinking' stokeslet. *J. Eng. Math.* 30 (1996) 151–168.
33. N. Liron and J.R. Blake, Existence of viscous eddies near boundaries. *J. Fluid Mech.* 107 (1981) 109–129.
34. K.B. Ranger, Eddies in two dimensional Stokes flow. *Int. J. Engng Sci.* 18 (1980) 181–190.
35. A. Avudainayagam and B. Jothiram, No-slip images of certain line singularities in a circular cylinder. *Int. J. Engng Sci.* 25 (1987) 1193–1205.
36. J.M. Dorrepaal, M.E. O'Neill and K.B. Ranger, Two-dimensional Stokes flows with cylinders and line singularities. *Mathematika* 31 (1984) 65–75.
37. A. Avudainayagam and B. Jothiram, A circle theorem for plane Stokes flows. *Q. Jl. Mech. Appl. Math.* 41 (1988) 383–393.
38. S.K. Sen, Circle theorems for steady Stokes flow. *J. Appl. Math. Phys.* (ZAMP) 40 (1989) 139–146.
39. J.H. Michell, The inversion of plane stress. *Proc. Lond. Math. Soc.* 34 (1901) 134–142.
40. C. Pozrikidis, *Introduction to theoretical and computational fluid dynamics*. Oxford: Oxford University Press (1997) 876 pp.
41. D.J. Acheson, *Elementary fluid dynamics*. Oxford Applied Mathematics and Computing Science Series. Oxford: The Clarendon Press (1990) 397 pp.
42. M. Charles and J. Wilson, Fermentor design. In: B.K. Lydersen, N.A. D'Elia and K.L. Nelson (eds.), *Bioprocess Engineering: Systems, Equipment and Facilities*. John Wiley and Sons (1994), pp. 5–67.
43. M.A. Winkler, Problems in fermenter design and operation. In: M.A. Winkler (ed.), *Chemical Engineering Problems in Biotechnology*. Critical Reports on Applied Chemistry (1990) Vol. 29, pp. 215–350.